Nonlinear dynamics of gravity and matter creation in a cosmology with an unbounded Hamiltonian

Gursoy B. Akguc,[1] L. E. Reichl,[1] E. V. Derishev,[2] Vl. V. Kocharovsky,[2] and V. V. Kocharovsky[2,3]
[1]*Center for Studies in Statistical Mechanics and Complex Systems, The University of Texas at Austin, Austin, Texas 78712, USA*
[2]*Institute of Applied Physics of the Russian Academy of Science, Nizhny Novgorod, Russia*
[3]*Department of Physics and Institute for Quantum Studies, Texas A&M University, Texas 77843-4242, USA*
(Received 24 June 2004; published 20 December 2004)

Nonlinear dynamics and stability properties of a cosmological model of spatially homogeneous coupled gravity and matter fields is analyzed using methods of classical mechanics. The system exhibits regions of chaos and dramatic changes in structural stability as the strength of the coupling between the fields is varied. Numerical simulations suggest that Hamiltonian systems with structure appropriate for describing matter-gravity interaction constitute a new class of nonlinear systems with very unusual and rich dynamics.

DOI: 10.1103/PhysRevE.70.066210 PACS number(s): 05.45.−a, 47.52.+j, 98.80.Cq, 98.80.Jk

I. INTRODUCTION

A consistent formulation of the quantum field theory of gravity and matter fields, and a simplified model of quantized conformally-flat gravity conformally coupled to a massive scalar field, was proposed in [1]. The Lagrangian of this model has the form

$$L = -\frac{1}{2}(-\psi^{,\mu}\psi_{,\mu} + m_\psi^2\psi^2) + \frac{1}{2}(-\phi^{,\mu}\phi_{,\mu} + m_\phi^2\phi^2) - \frac{1}{4!}\lambda_\psi\psi^4 + \frac{1}{4!}\lambda_\phi\phi^4 - \frac{1}{2\,!\,2!}\lambda\psi^2\phi^2, \tag{1}$$

in a Minkowski space-time with a metric $\eta_{\mu\nu}=\mathrm{diag}(1,-1,-1,-1)$, μ, $\nu=0,1,2,3$. Here $\psi=\Omega\Psi$, where the field Ψ describes the matter field with a mass m and a self-interaction coupling constant λ_ψ, ϕ is the gravity field (the scaled conformal factor of the spacetime metric tensor $g_{\mu\nu}=\Omega^2\eta_{\mu\nu}$, $\phi=(3/4\pi G)^{1/2}\Omega$), $\lambda=8\pi G m^2/3$, and $\lambda_\phi=-16\pi G\Lambda/3$, where G is the universal gravitational constant and Λ is the cosmological constant (for a general reference see, for example [2,3]).

We will study the stability of the classical (not quantum) dynamics imposed by this Lagrangian. We will restrict ourselves to the simple cosmological (minisuperspace) model where the fields are spatially homogeneous and only consider the variation of the amplitudes of the fields as a function of time. This will give valuable information about the long-wavelength stability of spatially varying fields. Since the fields are spatially homogeneous, we can simplify notation. If we let $\psi=x$ and $\phi=y$, we can write the Lagrangian in the form

$$L = -\frac{1}{2}(-\dot{x}^2 + m_x^2x^2) + \frac{1}{2}(-\dot{y}^2 + m_y^2y^2) - \frac{1}{24}\lambda_x x^4 + \frac{1}{24}\lambda_y y^4 - \frac{1}{4}\lambda x^2y^2, \tag{2}$$

where $\dot{x}=dx/dt$ and $\dot{y}=dy/dt$. The canonical momenta are defined $p_x=\partial L/\partial\dot{x}$ and $p_y=\partial L/\partial\dot{y}$ and the Hamiltonian is defined $H'=p_x\dot{x}+p_y\dot{y}-L$. This allows us to write the following Hamiltonian for the field amplitudes:

$$H' = \frac{1}{2}(p_x^2 + kx^2) - \frac{1}{2}(p_y^2 + ky^2) + \frac{a}{4}x^4 - \frac{b}{4}y^4 + \frac{c}{2}x^2y^2 = 0, \tag{3}$$

where we have chosen $m_x^2=m_y^2=k$, $\lambda_x=6a$, $\lambda_y=6b$, and $\lambda=2c$. A distinctive feature of this Hamiltonian is that it is unbounded from below as well as from above. The reason for that is that the y-oscillator contributes with the negative kinetic and potential energies to the total energy of the system. We analyze here the case when k, a, b, and c are positive constants. When $c=0$ the uncoupled x- and y-oscillators are stable anharmonic oscillators. Simultaneous creation of the matter and gravity, i.e., the cosmological birth and growth of the Universe, occurs only due to the nonlinear coupling ($c>0$) of the matter and gravity oscillators. The Hamiltonian is set equal to zero, $H=0$, which is a constraint imposed by the general theory of relativity in order to get the proper classical Einstein equations.

Within a semiclassical analysis of quantum gravity and matter interactions, the fact that the conformal factor of the spacetime metric contributes with a negative kinetic energy to the total Hamiltonian has been known for a long time [4–8]. Within a classical, nonquantized theory, a Hamiltonian system with a similar structure has been studied in [9–13] to describe a Friedmann-Robertson-Walker universe conformally coupled to a real, self-interacting, massive scalar field. For that case, $k=+1$ ($k=-1$) corresponds to a positive (negative) spatial curvature. For a particular case $a=b=0$, it was demonstrated in [9] how homoclinic chaos arises out of the internal resonances between x and y. The homoclinic chaos for the case $a=0$, $b<0$, $c\neq 0$ was reported in [10]. These conclusions were confirmed in [11] and [12] where the equations for the primary fixed points of the dynamics for various choices of parameters, k, a, b, and c were derived. They focused on the dynamics for the case $k=1$, $b=a+2c$, $a>0$, $c<0$, and $b<0$, when the gravity-related y oscillator is unstable by itself, and found that the phase space had a mixture of chaotic and regular behavior.

Here we focus on the parameter region $c>0$, $a>0$, $b>0$, and $k\geqslant 0$ which is appropriate to the physical interpretation of the Hamiltonian in Eq. (3) as describing the birth and cosmological evolution of the Universe in the process of the mutual creation of partially stable matter and gravity due to their nonlinear coupling. Furthermore, we set $b=a$ for the sake of simplicity since, probably, this particular case illustrates well enough the general case of different a and b if they are both positive. The Hamiltonian then takes the form

$$H=\frac{1}{2}(p_x^2+kx^2)-\frac{1}{2}(p_y^2+ky^2)+\frac{a}{4}(x^4-y^4)+\frac{c}{2}x^2y^2=0. \tag{4}$$

Hamilton's equations of motion can now be written as

$$\dot{x}=\frac{\partial H}{\partial p_x}=p_x, \quad \dot{p}_x=-\frac{\partial H}{\partial x}=-kx-ax^3-cxy^2,$$

$$\dot{y}=\frac{\partial H}{\partial p_y}=-p_y, \quad \dot{p}_y=-\frac{\partial H}{\partial y}=ky+ay^3-cx^2y. \tag{5}$$

It is useful to write the equations of motion as coupled second order differential equations for x and y,

$$\ddot{x}+kx+ax^3+cxy^2=0, \quad \ddot{y}+ky+ay^3-cx^2y=0. \tag{6}$$

The gravity-matter interaction ($c\neq 0$) affects the matter field and the gravity field in quite different ways. We will see this in the Poincaré surfaces of section and oscillograms $x(t)$ and $y(t)$ described below.

A first step in analyzing the behavior of the system is to find the primary fixed points of Hamilton's equations [15]. We look for sets of points (p_x^*,p_y^*,x^*,y^*) in phase space such that $(\dot{p}_x=0,\dot{p}_y=0,\dot{x}=0,\dot{y}=0)$. There are four sets of fixed points, (p_x^*,p_y^*,x^*,y^*). They are (0,0,0,0), $(0,0,\pm\sqrt{-k/a},0)$, $(0,0,0,\pm\sqrt{-k/a})$, and $[0,0,\pm\sqrt{k(c-a)/(a^2+c^2)}, \pm\sqrt{-k(a+c)/(a^2+c^2)}]$. For our system, all fixed points contain imaginary terms except for $(p_x^*,p_y^*,x^*,y^*)=(0,0,0,0)$ which is an elliptic (stable) fixed point. Since phase space coordinates must be real, this is the only primary fixed point for this system. This behavior of the primary fixed points causes the dynamics of the system considered here to be quite different from the conventional oscillator system discussed in [16,17], or the coupled gravity-matter system considered in [11–14].

The primary purpose of the present paper is to demonstrate, numerically, the impressive nonlinear dynamics generated by systems with the unbounded Hamiltonians, such as the one in Eq. (4). We discuss also a wide range of parameters for which the system (4) generates very interesting unstable solutions which, contrary to the stable (bounded) solutions, approach infinity (in most cases in an explosive fashion in a finite interval of the conformal time).

II. STABILITY OF MOTION IN PHASE SPACE

Information about the stability of this system is given in Fig. 1 which is a course-grained stability diagram of phase space trajectories for parameters $k=1$, $0.0137\leqslant a\leqslant 0.135$, and $0\leqslant c\leqslant 1.5$. The black squares each contain a trajectory that is stable (bounded). The white squares each contain a trajectory which is unstable (unbounded). All trajectories used to obtain Fig. 1 had initial conditions $(p_x,p_y,x,y)=(d,d,0,0)$, where $d=10$. The numerical criterion for instability of a trajectory was that it reach values of x and/or y such that $x^2+y^2\geqslant 10^7$. Generally, if a trajectory is unstable, the instability occurs very rapidly after some initial time interval $0<t<t_{\rm esc}$. Before the time $t=t_{\rm esc}$, the trajectory appears to be stable and remains at small values of x and y. After the time $t=t_{\rm esc}$ unstable trajectories appear to diverge exponentially or even explosively rapidly.

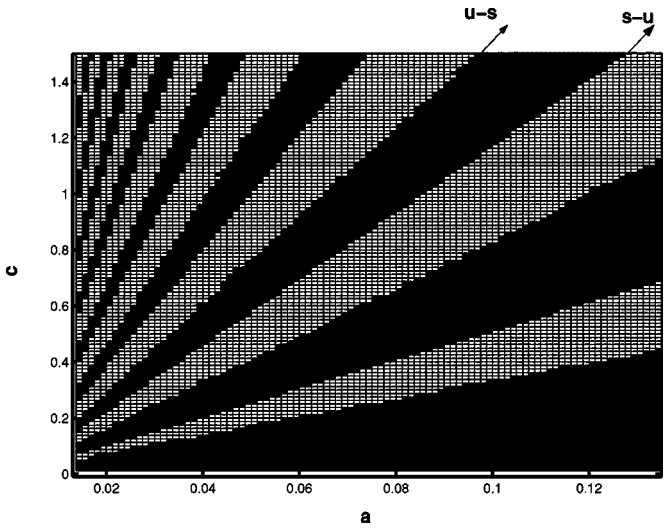

FIG. 1. A coarse-grained plot of stable and unstable regions as a function of parameters a and c. Black squares contain one stable trajectory and white squares contain one unstable trajectory. In all cases the initial conditions were $(p_x,p_y,x,y)=(d,d,0,0)$ with $d=10$.

Because there is an elliptic fixed point at the origin ($p_x=p_y=x=y=0$), there will always be a small stable harmonic region in the immediate neighborhood of the origin. (Within the original quantum theory of this minisuperspace model, the latter implies that the initially small vacuum spontaneous fluctuations of matter and gravity have to tunnel through a finite barrier in order to give birth and subsequent inflation of the Universe to a macroscopic state.) As we will see below, there generally are additional complex stable regions outside the harmonic regions. In the unstable regions in Fig. 1, much of the complex stable region disappears. For very small values of a (and fixed c) it becomes more and more difficult to resolve stable and unstable regions because, as we will see, the phase space becomes more and more complex with decreasing values of a.

In Fig. 2, we show the dependence of $t_{\rm esc}$ on the parameter d, which determines the initial values of the momenta for $k=1$, $c=0.8$, and $a=0.2375$ in the unstable region. If we start a trajectory farther away from the phase space origin, the escape time $t_{\rm esc}$ tends to be shorter. Although we only show the behavior of $x(t)$, the other phase space coordinates $y(t)$, $p_x(t)$, and $p_y(t)$ also diverge. In Fig. 3, we show $x(t)$ for $k=1$, $c=0.8$, and $a=0.2375$ and two initial conditions $d=5.9$ and $d=5.95$ which are closer to the origin. For these values

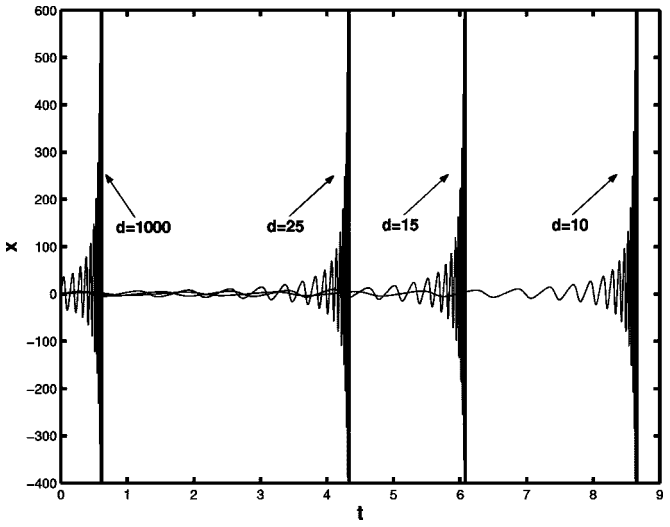

FIG. 2. The value of $x(t)$ as a function of time is shown for $a=0.2375$ and $c=0.8$ for initial conditions $(p_x,p_y,x,y)=(d,d,0,0)$ with $d=10$, 15, 25, and 1000. Arrows indicate the value of d for each curve. The escape time, for the cases considered, decreases with increasing d.

of k, a, and c, the trajectory becomes stable for all values of d less than $d=5.95$. Figure 4(a) shows the stability regions for $k=1$, $0\leqslant a\leqslant 0.32$, and $c=0.8$ and Fig. 4(b) shows a magnification of stability regions for $k=1$, $0\leqslant a\leqslant 0.038$, and $c=0.8$. The stability regions become more fractured as a decreases and appear to have a fractal-like character.

III. POINCARÉ SURFACES OF SECTION

We can study the overall structure of flow in the phase space using Poincaré surfaces of section [15]. We solve Hamilton's equations of motion numerically and we construct two types of surface of section. To show the behavior

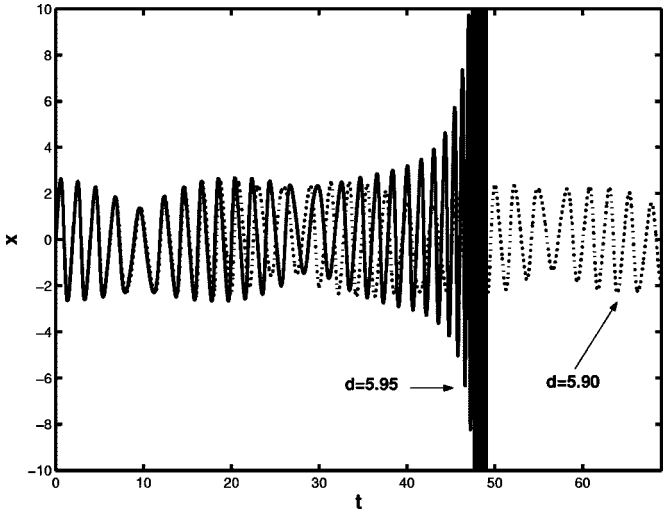

FIG. 3. The value of $x(t)$ as a function of time is shown for $a=0.2375$ and $c=0.8$ for initial conditions $(p_x,p_y,x,y)=(d,d,0,0)$ with $d=5.90$ and $d=5.95$. The trajectory with $d=5.90$ remains stable. The trajectory with $d=5.95$ is unstable.

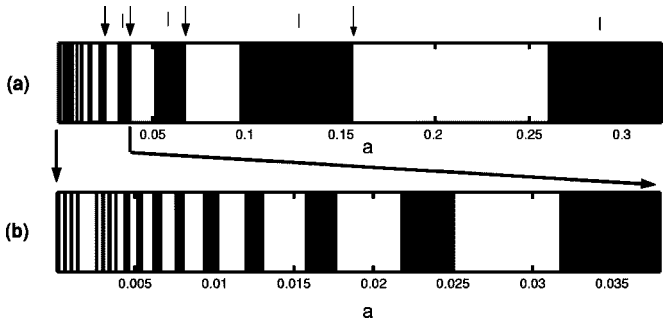

FIG. 4. Stable (black) and unstable (white) regions of the phase space for $c=0.8$ and varying values of the parameter a: (a) $0\leqslant a\leqslant 0.32$; (b) $0\leqslant a\leqslant 0.038$. The vertical lines (arrows) above (a) mark values of a for which surfaces of section are shown in Fig. 7 (Fig. 8).

of p_x and x we plot p_x versus x every time $y=0$ and $p_y>0$. To show the behavior of p_y and y we plot p_y versus y every time $x=0$ and $p_x>0$.

An important feature of this system is scale invariance. First, if we scale the canonical variables by a factor of $\sqrt{a}$, so that $\overline{x}=x\sqrt{a}$, $\overline{y}=y\sqrt{a}$, $\overline{p_x}=p_x\sqrt{a}$, and $\overline{p_y}=p_y\sqrt{a}$, then the equations of motion for scaled variables $(\overline{p_x},\overline{p_y},\overline{x},\overline{y})$ take the form

$$\dot{\overline{x}}=\overline{p_x},\quad \dot{\overline{p_x}}=-k\overline{x}-\overline{x}^3-\frac{c}{a}\overline{x}\,\overline{y}^2,$$

$$\dot{\overline{y}}=-\overline{p_y},\quad \dot{\overline{p_y}}=k\overline{y}+\overline{y}^3-\frac{c}{a}\overline{x}^2\overline{y}. \tag{7}$$

Second, if we scale the canonical variables and time according to $x\to\sqrt{|k|}\overline{x}$, $y\to\sqrt{|k|}\overline{y}$, $p_x\to|k|\overline{p_x}$, $p_y\to|k|\overline{p_y}$, $t\to t/\sqrt{|k|}$, then the equations of motion take the form

$$\dot{\overline{x}}=\overline{p_x},\quad \dot{\overline{p_x}}=-\operatorname{sgn}(k)\overline{x}-\overline{x}^3-\frac{c}{a}\overline{x}\,\overline{y}^2,$$

$$\dot{\overline{y}}=-\overline{p_y},\quad \dot{\overline{p_y}}=\operatorname{sgn}(k)\overline{y}+\overline{y}^3-\frac{c}{a}\overline{x}^2\overline{y}.$$

In other words, only a sign of k is important and it is enough to consider only three values $k=1,0,-1$.

Thus, along a line of fixed c/a on the (a,c) plane the equations of motion for the scaled variables are unchanged. As we change a and c keeping the ratio c/a constant, the structure of the phase space motion in terms of the original variables (p_x,p_y,x,y) will be unchanged, but its overall scale will change depending on how a is changed. This can be seen in Fig. 5, where we plot surfaces of section for $k=1$ and $c/a=0.075$, but for different values of a and c. Figures 5(a) and 5(b) show surfaces of section of p_x versus x and p_y versus y, respectively, for $(a=0.06,c=0.8,c/a=0.075)$. Figures 5(c) and 5(d) show surfaces of section of p_x versus x and p_y versus y, respectively, for $(a=0.6,\ c=8.0,\ c/a=0.075)$. The initial conditions (p_x^o,p_y^o,x^o,y^o) used to solve Hamilton's equations in Eq. (5) for all four plots are $(p_x^o=d/\sqrt{a},p_y^o=d/\sqrt{a},x^0=0,y^o=0)$ for $d\pm1,\pm5,\pm10,\pm20,\pm30,\pm40,$

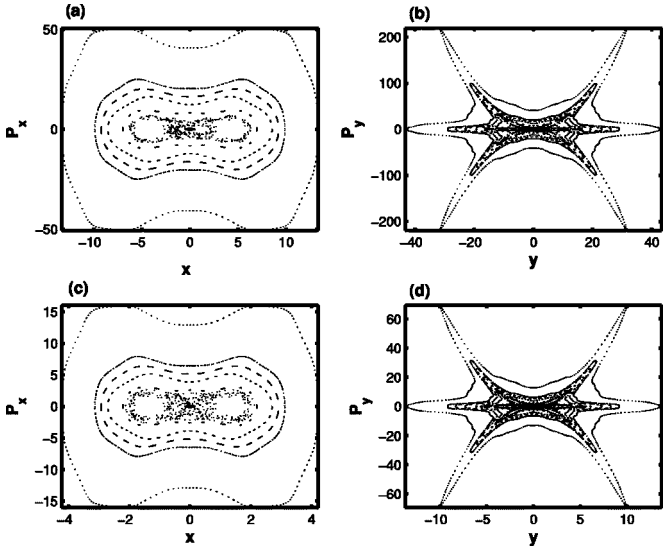

FIG. 5. Scaling behavior of the phase space. (a) p_x versus x surface of section for $a=0.06$ and $c=0.8$. (b) p_y versus y surface of section for $a=0.06$ and $c=0.8$. (c) p_x versus x surface of section for $a=0.6$ and $c=8.0$. (b) p_y versus y surface of section for $a=0.6$ and $c=8.0$. In all cases, the initial conditions were $(p_x^o=d/\sqrt{a}, p_y^o=d/\sqrt{a}, x^o=0, y^o=0)$ with $d=\pm1, \pm5, \pm10, \pm20, \pm30, \pm40, \pm50$, and ±100.

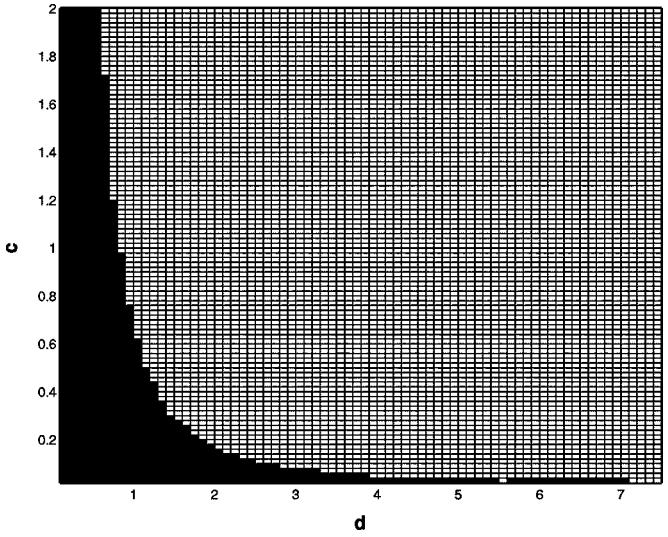

FIG. 6. A coarse-grained plot of stable and unstable regions (stability border) for $k=1, a=0$, as a function of initial conditions, d, and gravity-matter coupling strength, c. Black squares contain one stable trajectory and white squares contain one unstable trajectory.

$\pm50, \pm100$. We see that the surfaces of section are identical for Figs. 5(a) and 5(c) and for Figs. 5(b) and 5(d). However, the overall scale has changed by a factor of $\sqrt{0.6/0.06}=\sqrt{10}\approx3.16$. This scaling behavior is the reason we see stripes of stable and unstable motion along lines of constant c/a in Fig. 1. What is not clear is why the phase space alternates between stable and unstable behavior as we change the ratio c/a.

For the limiting case $a=b=0$ and arbitrary k, we can use an additional scaling $x\rightarrow\overline{x}/\sqrt{|c|}, y\rightarrow\overline{y}/\sqrt{|c|}, p_x\rightarrow\overline{p_x}/\sqrt{|c|}$, $p_y\rightarrow\overline{p_y}/\sqrt{|c|}$ that results in the equations of motion with c replaced by sgn(c). Combining it with the k-scaling law, we conclude that a stability border between stable (bounded) and unstable (unbounded) trajectories in the parameter space of initial conditions, d, gravity-matter coupling strength, c, and curvature k is determined by the scaling law $c=(k^2/d^2)c_{cr}$. Numerically we find from Fig. 6 that there is only one critical value of the gravity-matter coupling $c_{cr}\simeq0.61$ and the stability border, indeed, satisfies the above scaling law.

Another important feature of this system is that as we cross from one stable stripe to another in Fig. 1 qualitative changes occur in the structure of stable phase space flow. In Fig. 7, we show the p_x versus x and p_y versus y surfaces of section for $k=1$, $c=0.8$, and $a=0.29,0.13,0.06,0.036$. These values of a are indicated by the vertical lines above Fig. 4(a). The initial conditions in all cases are $d=\pm1, \pm5, \pm10, \pm20, \pm30, \pm40, \pm50, \pm100$. Note that each time we pass from one stable stripe to the next, in the direction of decreasing a, an additional set of spines gets added to the phase space structure in the p_y versus y surface of section. This process continues to the smallest values of a that we could resolve. The p_y versus y phase space structure for the stable stripe with the smallest values of c/a does not contain any spines. The p_y versus y phase space structures on stable stripes with very large values of c/a contain many spines.

It is interesting to see how the phase space structures in Figs. 7(b)–7(d) and 7(f)–7(h) change as we move to the right-hand edge of the stable stripe that they inhabit. In Fig. 8, we show the p_x versus x and p_y versus y surfaces of section for $k=1$, $c=0.8$, and $a=0.156$, 0.066, 0.0375, and 0.024. The initial conditions used are again $d=\pm1, \pm5, \pm10, \pm20, \pm30, \pm40, \pm50$, and ±100. All the structures are expanding into larger regions of the phase space. If we change the value of c/a by a small amount and pass into the unstable region on the right, all the phase space structure disappears except for a tiny island around the primary fixed point at $(p_x^*, p_y^*, x^*, y^*)=(0,0,0,0)$. Note that the p_y versus y phase space structure in Fig. 8(h) lies on a stable stripe to the left of the one in Fig. 7(h) and it has an additional set of spines.

We can also look at the effect of the "curvature" parameter, k. In Fig. 9 we show surfaces of section of the phase space near the origin for the cases $k=0$ and $k=1$ with $a=0.06$ and $c=0.8$. For $k=0$ only regular trajectories occur near the origin, at least on the large scale shown. However, with $k=1$ a stochastic web [18] appears to form in the neighborhood of the origin.

IV. STABLE AND UNSTABLE FIXED POINTS FOR PARTIAL HAMILTONIANS

It is interesting to consider the decomposition of the Hamiltonian into partial Hamiltonians which contain individual resonance contributions, similar to the approach of Walker and Ford [19]. We can perform a canonical transformation from the Cartesian coordinates (p_x, p_y, x, y) to action-angle coordinates $(J_x, J_y, \theta_x, \theta_y)$. The Hamiltonian then takes the form

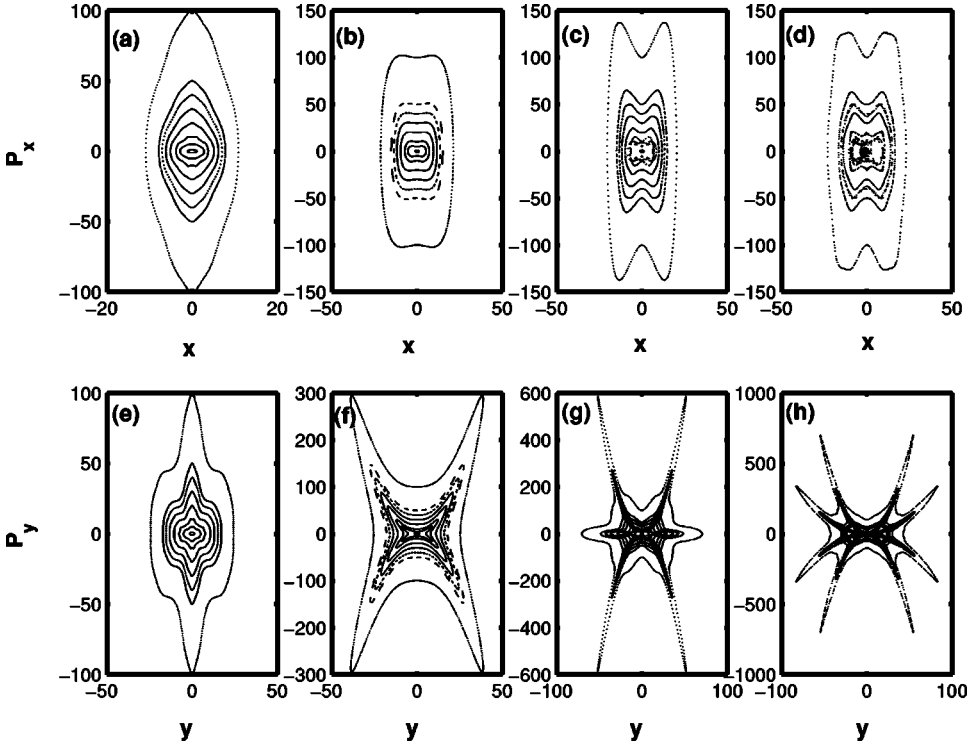

FIG. 7. Surfaces of section p_x versus x for $c=0.8$ and (a) $a=0.29$, (b) $a=0.13$, (c) $a=0.06$, and (d) $a=0.036$. Surfaces of section p_y versus y for $c=0.8$ and (e) $a=0.29$, (f) $a=0.13$, (g) $a=0.06$, and (h) $a=0.036$. These values of a occur at points in Fig. 4(a) which are marked by vertical lines. In all cases, the initial conditions were $(p_x^o=d, p_y^o=d, x^o=0, y^o=0)$ with $d=\pm1, \pm5, \pm10, \pm20, \pm30, \pm40, \pm50$, and ±100.

$$H(J_x, J_y, \theta_x, \theta_y) = H_o + V_{(2,0)}\cos(2\theta_x) + V_{(0,2)}\cos(2\theta_x) + V_{(4,0)}\cos(4\theta_x) + V_{(0,4)}\cos(4\theta_y) + V_{(2,2)}\cos(2\theta_x + 2\theta_y) + V_{(2,-2)}\cos(2\theta_x - 2\theta_y) = 0, \tag{8}$$

where the angle independent part of the Hamiltonian is

$$H_o = J_x - J_y + \frac{3a}{8}(J_x^2 - J_y^2) + \frac{c}{2}J_xJ_y \tag{9}$$

and the coefficients of the resonance terms are given by

$$V_{(2,0)} = \frac{a}{2}J_x^2 + \frac{c}{2}J_xJ_y, \quad V_{(0,2)} = -\frac{a}{2}J_y^2 + \frac{c}{2}J_xJ_y,$$

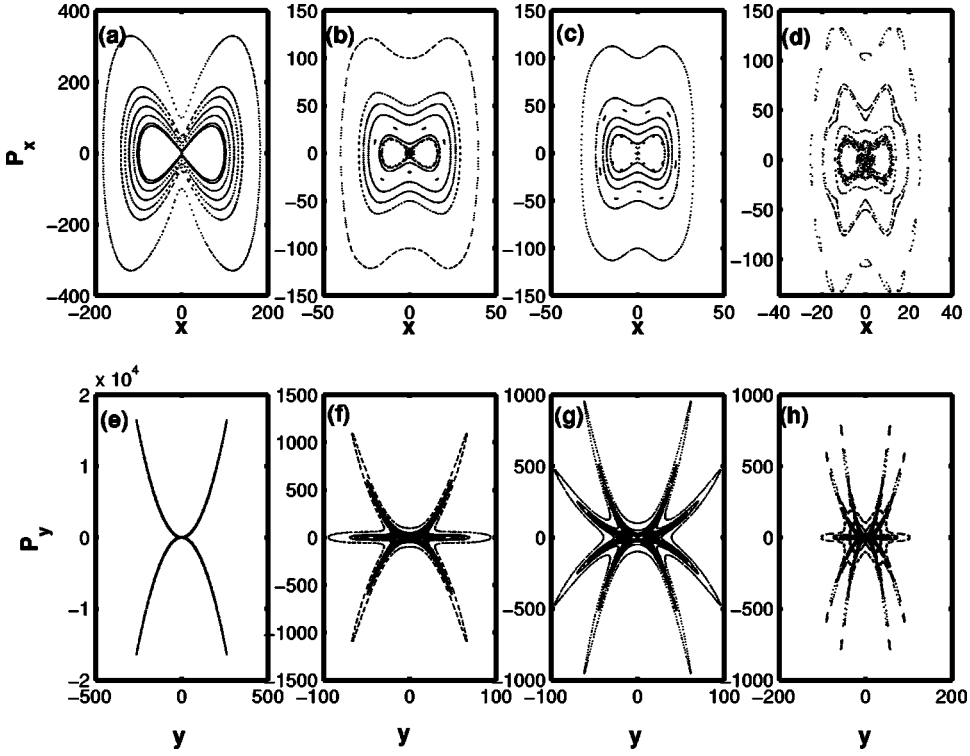

FIG. 8. Surfaces of section p_x versus x for $c=0.8$ and (a) $a=0.156$, (b) $a=0.066$, (c) $a=0.0375$, and (d) $a=0.024$. Surfaces of section p_y versus y for $c=0.8$ and (e) $a=0.156$, (f) $a=0.066$, (g) $a=0.0375$, and (h) $a=0.024$. These values of a occur at points in Fig. 4(a) which are marked by arrows. In all cases, the initial conditions were $(p_x^o=d, p_y^o=d, x^o=0, y^o=0)$ with $d=1$, 5, 10, 20, 30, 40, 50, and 100.

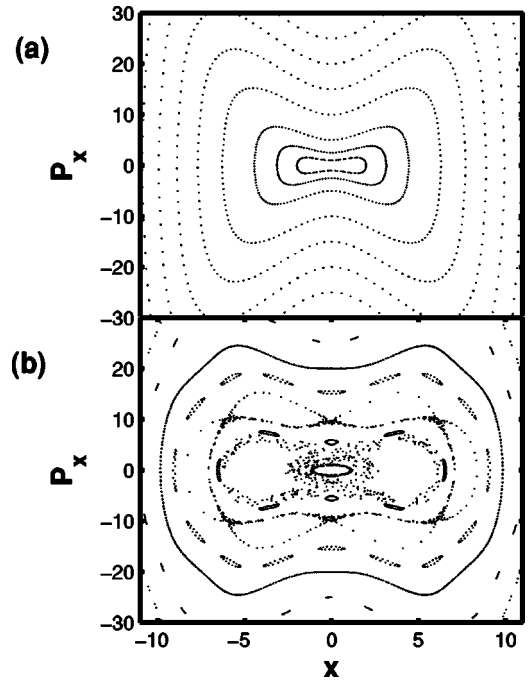

FIG. 9. (a) Surface of section of p_x versus x for $k=0$, $a=0.06$, and $c=0.8$. (b) Surface of section of p_x versus x for $k=1$, $a=0.06$, and $c=0.8$.

$$V_{(4,0)} = \frac{a}{8}J_x^2, \quad V_{(0,4)} = -\frac{a}{8}J_y^2, \quad V_{(2,2)} = \frac{c}{4}J_xJ_y,$$

$$V_{(2,-2)} = \frac{c}{4}J_xJ_y. \tag{10}$$

Following the Walker-Ford approach, we show phase space plots for each of the six Hamiltonians

$$H_{(n_x,n_y)} = H_o + V_{(n_x,n_y)}\cos(n_x\theta_x + n_y\theta_y) = 0, \tag{11}$$

where $(n_x,n_y)=(2,0),(0,2),(4,0),(0,4),(2,2),(2,-2)$. Each of these Hamiltonians is integrable. Only the Hamiltonians $H_{(2,0)}$ and $H_{(0,2)}$ appear to give rise to nontrivial phase space behavior. For $H_{(2,0)}$, J_y is a constant of the motion. A phase space plot of p_x versus x is shown in Fig. 10(a) for $c=0.8$ and $a=0.06$. This system has primary hyperbolic fixed points at $(J_x=4/a,\theta=\pi/2)$ and $(J_x=4/a,\theta=3\pi/2)$. No phase space orbits exist for large values of $p_x>\sqrt{8/a}$. For $H_{(0,2)}$, J_x is a constant of the motion. A phase space plot of p_y versus y is shown in Fig. 10(b) for $c=0.8$ and $a=0.06$. This system has primary elliptic fixed points at $(J_x=4/a,\theta=\pi/2)$ and $(J_x=4/a,\theta=3\pi/2)$. Surfaces of sections for the remaining Hamiltonians are plotted in Figs. 10(c)–10(f) for $c=0.8$ and $a=0.06$. These remaining Hamiltonians have no nontrivial primary fixed points and exhibit very regular behavior. In Figs. 11(a) and 11(b) we plot the p_x versus x and p_y versus y surfaces of section for the full Hamiltonian for $c=0.8$ and $a=0.06$. It is clear that the full phase space is much more complicated than its individual parts. Even for very small values of a and c we were not able to find a regime where the full dynamics clearly showed the contributions from its individual parts, as was the case for the system considered by Walker and Ford. This suggests that the systems with the unbounded Hamiltonians, for example the model (4)–(6) considered in the present paper, constitute an unusual class of the dynamical systems.

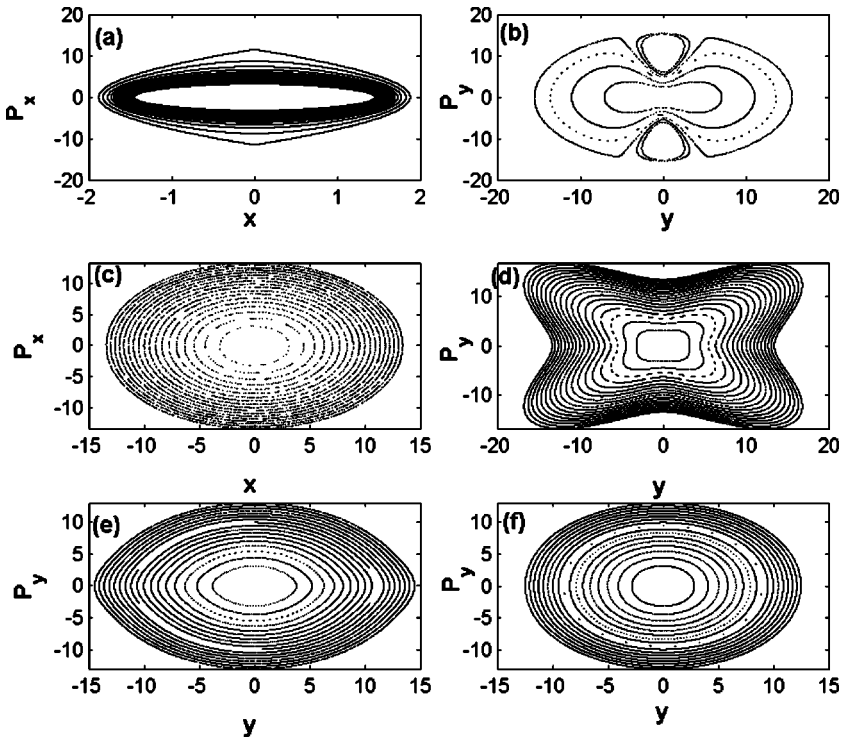

FIG. 10. Phase space plots for the six Hamiltonians $H_{(n_x,n_y)}$ for $c=0.8$ and $a=0.06$. (a) A plot of p_x versus x for $H_{(2,0)}$. (b) A plot of p_y versus y for $H_{(0,2)}$. (c) A plot of p_x versus x for $H_{(4,0)}$. (d) A plot of p_y versus y for $H_{(0,4)}$. (e) A plot of p_y versus y for $H_{(2,2)}$. (f) A plot of p_y versus y for $H_{(2,-2)}$.

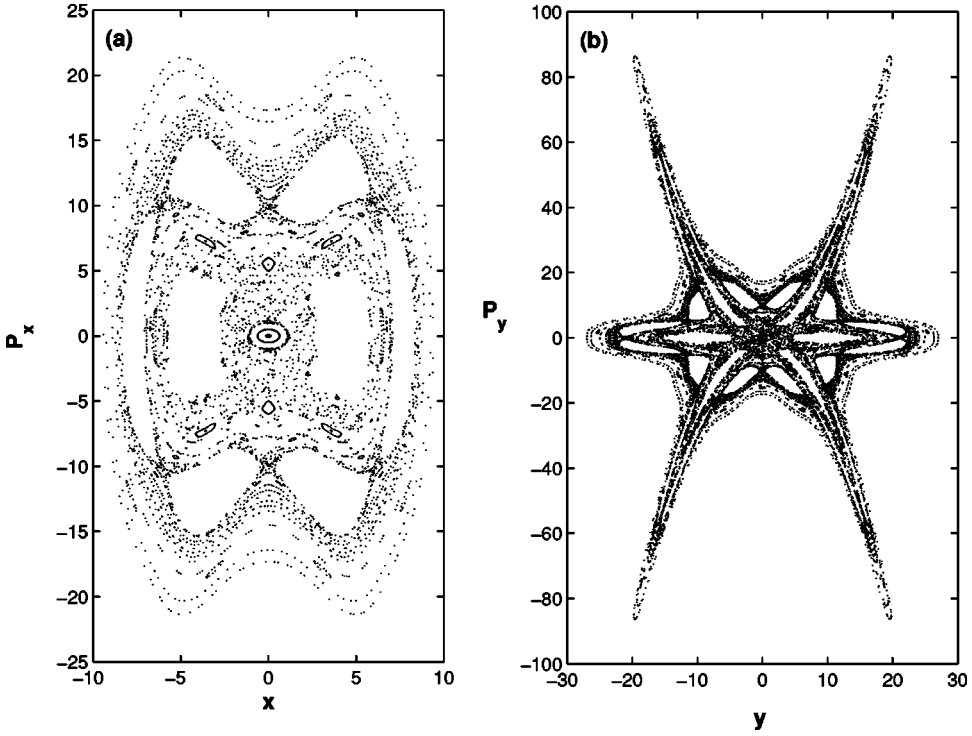

FIG. 11. Surfaces of section for the full Hamiltonian for $a=0.06$ and $c=0.8$. (a) p_x versus x. (b) p_y versus y.

V. INTERVALS OF ADIABATIC MOTION

We have found that for $a=0$ and $a \ll c$, some of the behavior of unstable x and y oscillations can be understood in terms of an adiabatic analysis. In Figs. 12(a) and 12(b), we plot $x(t)$ versus t and $y(t)$ versus t, for the early times, for $k=1$, $a=0$, $d=1.9$, and $c=0.8$. In Figs. 12(c) and 12(d), we plot $x(t)$ versus t and $y(t)$ versus t for $k=1$, $a=0.0015$, $d=1.9$, and $c=0.8$. We see some distinctive differences in the behavior for $a=0$ and for $a=0.0015$. For $a=0$, the period of the y oscillations is approximately constant and the maximum amplitude of the y oscillations can increase or decrease with increasing time. The x oscillations have very small amplitude relative to those of the y oscillator, and they have a very short period that appears to depend inversely on the amplitude of the y oscillations. For $a=0.0015$, the period of the y oscillations can vary and appears to depend on the amplitude of the y oscillations. Also, both the amplitude and period of the x oscillations appears to depend on the amplitude of the y oscillations.

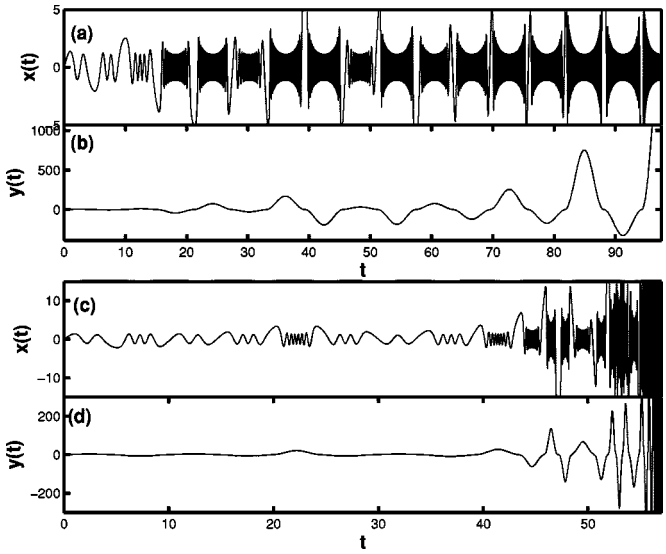

FIG. 12. (a) Plot of $x(t)$ versus t and (b) $y(t)$ versus t for $k=1$, $a=0$, $d=1.9$, and $c=0.8$. (c) Plot of $x(t)$ versus t and (d) $y(t)$ versus t for $k=1$, $a=0.0015$, $d=1.9$, and $c=0.8$.

We can understand some of the behavior in Fig. 12 using the theory of the adiabatic invariants [20]. Let us write $y(t)=\overline{y}(t)+\Delta y(t)$, where $\Delta y(t)$ is assumed small, $\overline{y}(t)$ is defined

$$\overline{y}(t) = \frac{1}{T_x(t)} \int_0^{T_x(t)} y(t)\, dt, \tag{12}$$

and $T_x(t)$ is the period of the x oscillator at time t. We assume that $T_x(t)$ is a very slowly varying function of time and does not change significantly during one period of the x oscillation. Let us also write $x(t)=\overline{x}(t)+\Delta x(t)$, where $\Delta x(t)$ is assumed small and

$$\overline{x}(t) = X(t)\sin\left[\int^t \Omega_x(t)dt + \phi\right], \tag{13}$$

with $X(t)$ a slowly varying function of t. If we substitute Eq. (13) into Eq. (6) for $x(t)$ and average over one period, $T_x(t)$, we obtain

$$-\Omega_x^2(t)X(t) + kX(t) + \frac{a}{2}X^3(t) + c\overline{y^2}(t)X(t) = 0. \tag{14}$$

Thus the frequency of the x oscillator can be written as

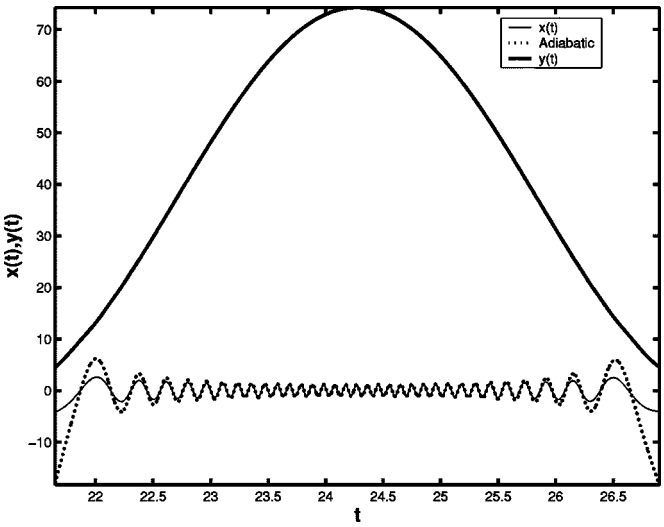

FIG. 13. Plot of $x(t)$ and $y(t)$ versus t for an oscillation interval in Figs. 12(a) and 12(b) (for $k=1$, $a=0$, $d=1.9$, and $c=0.8$).

$$\Omega_x^2(t) = k + \frac{a}{2}X^2(t) + c\overline{y^2}(t), \tag{15}$$

which is a slowly varying function of t. In Fig. 13, we plot $x(t)$ versus t and $y(t)$ versus t for an interval of oscillations in Fig. 12(a). In the region where $y(t)$ is large enough to ensure the condition of the adiabatic approximation $|\dot{\Omega}_x| \ll \Omega_x^2$, the agreement is excellent.

Because both $X(t)$ and $\Omega_x(t)$ are slowly varying functions of time, the adiabatic invariant $\Omega_x(t)X^2(t)$ of the x oscillator is approximately conserved during the time interval over which this adiabatic approximation applies. Let $y_{\max}=A$ denote the maximum value of the y-oscillator amplitude, and let $X_{\min}$ denote the minimum value of the x-oscillator amplitude. Then the approximate conservation of the adiabatic invariant gives

$$X^2(t)\sqrt{k + \frac{a}{2}X(t)^2 + c\overline{y^2}(t)} = X_{\min}^2\sqrt{k + \frac{a}{2}X_{\min}^2 + cA^2}. \tag{16}$$

For $k=1$ and small a and $X(t)$, this becomes

$$X(t) \approx X_{\min}\sqrt{\frac{A}{\overline{y}(t)}}. \tag{17}$$

Thus, as $\overline{y}(t)$ decreases away from its maximum value, the amplitude of the x oscillations increases as can be seen in Fig. 12.

It is useful to substitute these expressions into the Hamiltonian in Eq. (4) for $y(t)$ at its maximum amplitude where $\dot{y}(t)=0$ and average over one period of oscillation of the x oscillator. We then find

$$X_{\min}^2 = \frac{1}{c}\left[k + \frac{a}{2}A^2\right]. \tag{18}$$

Thus for $a=0$ the minimum amplitude of the x oscillator is always the same, but for $a\neq 0$ the minimum value of x-oscillator amplitude depends on the maximum amplitude of the y oscillator. This variation of $X_{\min}$ with A can be seen in Fig. 12(c).

After each interval of adiabatic motion, the system undergoes a relatively short interval of nonadiabatic motion where $y(t)$ approaches and crosses zero. During the nth nonadiabatic interval, the adiabatic approximation $|\dot{\Omega}| \ll \Omega^2$ is violated, and the x oscillator acquires an additional phase shift $\Delta\phi_n$ so that its phase ϕ at the next, $(n+1)$th interval of adiabatic motion becomes $\phi_{n+1}=\phi_n+\Delta\phi_n$. The amplitude of the y oscillator is also changed from A_n to a different value A_{n+1} that, for large enough A, results in a very large change of the integral adiabatic phase shift $\int^t \Omega_x(t)dt \gg \pi$ at the $(n+1)$th interval of adiabatic motion compared to the nth interval. Since the result of the nonadiabatic transformation $A_n \rightarrow A_{n+1}$, $\phi_n \rightarrow \phi_{n+1}$ strongly depends on the phase with which the x oscillator enters the nonadiabatic region of motion, the system turns out to be very sensitive to any small perturbations in the phase space. The latter may explain qualitatively one of the possible mechanisms of the dynamical chaos in the system.

VI. COSMOLOGICAL EVOLUTION IN TERMS OF THE OBSERVABLE TIME AND GENERAL OVERVIEW

The purpose of this section is to sketch how the dynamics of the models in Eq. (1) or (2) can be translated into cosmology. Analysis of the regimes describing an observable cosmological evolution will be given elsewhere.

The model described in previous sections gives a classical picture of a cosmological evolution of our Universe as a self-consistent process of mutual creation of the interacting gravity and matter fields from originally small quantum fluctuations. The model only describes a classical stage of the evolution when both fields have reached the macroscopic coherent values. Justification of the classical model and description of the preceding spontaneous fluctuations can be made on the basis of the full quantum equations of the quantum field model (1) in a direct analogy with a well known theory (quantum electrodynamics in a cavity) of the laser radiation that starts from spontaneous quantum fluctuations and, due to stimulated amplification, very soon reaches the classical (often called as semiclassical) regime with a macroscopically large (coherent) field amplitude [21]. Moreover, the model (4)–(6) assumes that both fields are spatially homogeneous. Subsequent or simultaneous creation of all other spatial modes of the scalar and other matter fields, for example incoherent components of matter and radiation, could alter cosmological evolution, especially near singularities [13]. In particular, the process of reheating of the Universe due to decay and dissipation of the coherent inflation scalar field into incoherent matter and radiation as well as the processes of spontaneous quantum creation of particles from a vacuum due to various nonadiabatic mechanisms in a nonstationary curved spacetime (e.g., like Hawking radiation near black holes) [2] could become important at some stage [3]. Obviously, all such effects should be treated on the basis of a full quantum field theory of the model (1) or of the more

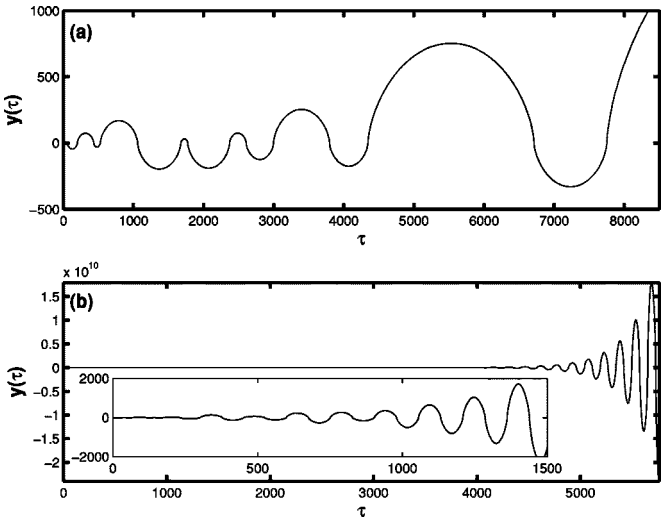

FIG. 14. (a) Plot of $y(\tau)$ versus τ for $k=1$, $a=0$, $d=1.9$, and $c=0.8$. (b) Plot of $y(\tau)$ versus τ for $k=1$, $a=0.0015$, $d=1.9$, and $c=0.8$. The inset shows more details of the early time behavior.

general models and are beyond the scope of the present minisuperspace model (4)–(6).

The behavior of the model (4)–(6), so far, has only been studied in terms of the conformal time, t. In order to relate the predictions of the model with the observational cosmology, one has to use the well-known relations [2]

$$\tau = \int_0^t |\Omega(t)|dt = \sqrt{\frac{4\pi G}{3}} \int_0^t |y(t)|dt \tag{19}$$

between the conformal time t and the observable time τ. They stem from the Friedmann-Robertson-Walker representation for a line element, $(ds)^2=\Omega^2(t)(dt)^2=(d\tau)^2$, in the conformally-flat spacetime $g_{\mu\nu}=\Omega^2\eta_{\mu\nu}$ and for the spatially homogeneous fields that we consider here.

For the case $a\neq 0$, it is of interest to plot the gravity field (the "radius" of the Universe) $y(\tau)$ versus τ rather than $y(t)$ versus t, as was done in Fig. 12. In Fig. 14(a) we plot $y(\tau)$ versus τ for $k=1,a=0,c=0.8,d=1.9$ [the same case as Fig. 12(b)]. In Fig. 14(b) we plot $y(\tau)$ versus τ for $k=1,a=0.0015,c=0.8,d=1.9$ [the same case as Fig. 12(d)]. We see that, while in the $y(t)$ versus t plot in Fig. 12(d) the y oscillations with larger amplitude have shorter periods, in the $y(\tau)$ versus τ plot in Fig. 14(b), these same y oscillations have approximately constant period.

The conformal field $\Omega(t)$, i.e., the y oscillator $y=(3/4\pi G)^{1/2}\Omega$, plays the part of an overall scale factor in the Universe that stretches the observable time τ with respect to the conformal time t. As a reference regime, let us consider a regime of the explosive evolution of the conformal factor

$$\Omega(t) = [(t_\infty - t)h]^{-1} \tag{20}$$

that ends in a singularity at a finite moment of the conformal time t_∞ [$y(t)\to\infty$ as $t\to t_\infty$] and corresponds to a standard de Sitter inflation

$$\Omega(\tau) = \Omega_0 \exp(h\tau), \quad \Omega_0 = (ht_\infty)^{-1}, \tag{21}$$

over an infinite interval of the observable time with a constant Hubble parameter

$$h = \frac{1}{\Omega}\frac{d\Omega}{d\tau} = \frac{1}{\Omega^2}\frac{d\Omega}{dt}. \tag{22}$$

Therefore, if the model has solutions which are not stabilized dynamically at some finite level but appear to end in the singularities, these singular solutions can have a well-defined physical meaning in the Friedmann-Robertson-Walker representation and, in fact, are of great importance for they describe the observable cosmological inflation. The end of the conformal time at $t=t_\infty$, e.g., in the de Sitter regime when

$$t = \int_0^\tau \frac{d\tau}{|\Omega(\tau)|} = \frac{1}{h\Omega_0}(1-e^{-h\tau}) \to t_\infty = \frac{1}{h\Omega_0} \quad \text{at } \tau \to +\infty, \tag{23}$$

implies a well-known fact that an event horizon

$$R_e(t) = |\Omega(\tau)| \int_\tau^\infty d\tau' / |\Omega(\tau')| = |\Omega(t)|(t_\infty - t), \tag{24}$$

i.e., the distance in the Universe from which the light could bring to us an information about the events taking place at the moment τ, can be finite, e.g., of the order of $1/h$, that imposes a finite upper bound on the size of the observable part of the Universe. At the same time, a particle horizon

$$R_p(t) = |\Omega(\tau)| \int_0^\tau d\tau' / |\Omega(\tau')| = |\Omega(t)|t, \tag{25}$$

i.e., an actual distance travelled by light from the initial moment of big bang until the present moment of time $\tau(t)$ or, in other words, an actual size of the observable part of the Universe at the present moment of time, tends to infinity at $t\to t_\infty$ proportionally to the scale of the Universe $|\Omega(t)|\to\infty$.

Such explosive solutions seem arise naturally in the present model (2). It is obvious when $b<0$ and $a>0$ since in this case the gravity y oscillator is unstable by itself. However, when $b>0$ the explosive solutions take place due to the nonlinear interaction of the y oscillator (gravity) with the x oscillator (matter), even if the y oscillator is partially stable, $b>0$, i.e., the cosmological constant is negative, $\Lambda=-3\lambda_\phi/(16\pi G)<0$. A comparison with the reference explosive law of Eq. (20), that corresponds to the de Sitter inflation, demonstrates that the model in Eq. (1) has a potential to explain naturally cosmological inflation and simultaneously solve the problem of the cosmological constant.

The discussion above indicates that the unstable and explosive solutions are more interesting and closely related to the observational cosmology than the stable solutions. At the same time, the stable solutions which demonstrate chaotic bounded behavior are also interesting for they shed a light on how a newly borning Universe is "hesitating" and searching for a way out of a small scale phase-space region around the trivial zero fixed point to an inflationary large scale phase-space region.

It would be interesting to check whether an original quantum field model (1), that is much more involved than the classical minisuperspace model (4)–(6), could explain a transition from a decelerating regime to an accelerating regime of the Universe expansion that, according to recent astronomical observations [22], occurs at a redshift $z \sim 0.5$. This transition means that the observable acceleration $d^2|\Omega|/d\tau^2$ after being positive at the de Sitter–like inflation stage, should become negative for a finite interval of time and then should change its sign to a positive value again at the latest times.

A simple illustrative example shown in Fig. 14 is not of that complicated type since the second derivative $d^2|\Omega|/d\tau^2$ has the same sign on each interval of adiabatic motion that corresponds to the expansion of the Universe from zero size to some maximal radius ($y=A$) with a deceleration and then contraction of the Universe again to the zero size (big crunch) with an acceleration.

Other regimes which are more relevant to the observations are possible in this system as well. Of course, for the actual explanation and prediction of the cosmological evolution, along with the basic classical dynamics (4)–(6) of two oscillators the other essential properties of the original quantum field theory (1) have to be included in the analysis. Let us mention some of them. First, according to the renormalization-group analysis [1], the nonlinear coupling parameters λ, λ_ϕ, and λ_ψ, that is c, b, and a, are in fact the running constants which are the functions of the energy scale of the process (in particular, of the relative momentum $\dot{y}/y$). This feature effectively modifies the nonlinearities of the coupled anharmonic oscillators (4)–(6). It is especially important in the regions where the self-coupling parameter $\lambda_\phi = -16\pi G\Lambda/3$ changes its sign around zero value, i.e., for relatively small cosmological constant Λ, and in the infrared and ultra-violet asymptotically free regions where all nonlinear coupling parameters vanish (see details in [1]). Second, the explicitly quantum effects in the chaotic dynamics and averaging of the observable quantities, e.g., $\langle\Omega^2\rangle$, could be important. Third, the effects of the spatially inhomogeneous modes of the gravity and matter fields on the global nonlinear dynamics and instability could be also important. Some effects originated from an inclusion of one more spatial mode of the matter field in a similar model with $a=0, b<0$, $c>0, k>0$ was discussed in [13]. These and other effects in the original model (1), which were not included in the particular dynamical model (4)–(6), as well as a realistic cosmology based on the model (1) with the unbounded Hamiltonian will be discussed elsewhere.

The present simplified model (4)–(6) clearly demonstrates that the actual dynamics of the cosmological expansion is naturally more intriguing and rich than was assumed in most of the models used until recently for the interpretation of the astronomical observations in cosmology.

VII. CONCLUSIONS

The system we consider here has very different structure from the coupled nonlinear oscillator systems that one finds in nonrelativistic classical mechanics, even though the Hamiltonian at first sight has many similarities. A possible analogy is that of an anharmonic oscillator coupled to an external field whose strength is nonlinearly affected by the degree of excitation of the oscillator. The system has very unusual stability and dynamical properties. There are vast regions of parameter space where the system is only stable for very small values of the matter and gravity fields and demonstrates fast growth of fields to infinity in an explosive fashion. In other regions of parameter space, the system appears to be stable (bounded) regardless of the amplitude of the fields although it can undergo huge variations in the values of these fields. The main conclusion from the numerical analysis presented above is that the systems with the unbounded Hamiltonians constitute very interesting class of nonlinear systems with very unusual and rich dynamics.

ACKNOWLEDGMENTS

Authors G.B.A. and L.E.R. thank the Robert A. Welch Foundation (Grant No. F-1051) and the Engineering Research Program of the Office of Basic Energy Sciences at the U.S. Department of Energy (Grant No. DE-FG03-94ER14465) for support of this work. Author L.E.R. thanks the U.S. Office of Naval Research (Grant No. N00014-03-1-0639) for partial support of this work. Author E.V.D. acknowledges the support from the Russian Science Support Foundation. Authors E.V.D., Vl.V.K., and V.V.K. acknowledge the grant 1744.2003.2 of the Council for Support of the Leading Scientific Schools of the Russian Federation.

[1] V. V. Kocharovsky and Vl. V. Kocharovsky, Found. Phys. **26**, 243 (1996).
[2] N. D. Birell and P. C. W. Davies, *Quantum Fields in Curved Space* (Cambridge University Press, Cambridge, London, 1982).
[3] E. Kolb and M. Turner, *The Early Universe* (Addison-Wesley, New York, 1988).
[4] E. P. Tryon, Nature (London) **246**, 396 (1973).
[5] P. I. Fomin, Dokl. Akad. Nauk SSSR **A9**, 831 (1975).
[6] R. Brout *et al.*, Ann. Phys. (Paris) **115**, 78 (1978); Gen. Relativ. Gravit. **10**, 1 (1979); Nucl. Phys. B **170**, 228 (1980).
[7] E. Gunzig, J. Geheniau, and I. Prigogine, Nature (London) **330**, 621 (1987).
[8] E. Gunzig and P. Nardone, Fundam. Cosmic Phys. **11**, 835 (1989).
[9] E. Calzetta and C. El Hasi, Class. Quantum Grav. **10**, 1825 (1993).
[10] E. Calzetta, in *Deterministic Chaos in General Relativity*, edited by A. Burd, A. Coley, and D. Hobill (Plenum, New York, 1994).
[11] S. Blanco, G. Domenech, C. El Hasi, and O. A. Rosso, Gen. Relativ. Gravit. **26**, 1131 (1994).

[12] S. Blanco, A. Costa, and O. A. Rosso, Gen. Relativ. Gravit. **27**, 1295 (1995).
[13] E. Calzetta and C. El Hasi, Phys. Rev. D **51**, 2713 (1995).
[14] A. Helmi and H. Vucetich, Phys. Lett. A **230**, 153 (1997).
[15] Linda E. Reichl, *The Transition to Chaos: Conservative Classical Systems and Quantum Manifestations*, 2nd ed. (Springer-Verlag, New York, 2004).
[16] M. Lakshmanan and R. Sahadevan, Phys. Rev. A **31**, 861 (1985).
[17] M. Lakshmanan and R. Sahadevan, Phys. Rep. **224**, 1 (1993).
[18] G. M. Zaslavsky, M. Edelman, and B. A. Niyazov, Chaos **7**, 159 (1997).
[19] G. H. Walker and J. Ford, Phys. Rev. **188**, 416 (1969).
[20] L. D. Landau and E. M. Lifshitz, *Mechanics*, Course of Theoretical Physics Vol. 1 (Butterworth-Heinemann, Oxford, 2000).
[21] M. Sargent III, M. O. Scully, and W. E. Lamb, Jr., *Laser Physics* (Addison-Wesley, Reading, MA, 1974).
[22] A. G. Riess *et al.*, Astrophys. J. **607**, 665 (2004).